



# Mesenchymal stromal cells reprogram monocytes and macrophages with processing bodies

Hyunjung Min<sup>1,2</sup> | Li Xu<sup>1</sup> | Roberta Parrott<sup>1</sup> | Christopher C. Overall<sup>3</sup> |  
 Melina Lillich<sup>1</sup> | Emily M. Rabjohns<sup>4</sup> | Rishi R. Rampersad<sup>4</sup> | Teresa K. Tarrant<sup>4</sup>  |  
 Norin Meadows<sup>1</sup> | Anthony Fernandez-Castaneda<sup>3</sup> | Alban Gaultier<sup>3</sup> |  
 Joanne Kurtzberg<sup>1,5</sup> | Anthony J. Filiano<sup>1,2,6,7</sup> 

<sup>1</sup>Marcus Center for Cellular Cures, Duke University, Durham, North Carolina

<sup>2</sup>Department of Neurosurgery, Duke University, Durham, North Carolina

<sup>3</sup>Department of Neuroscience, Center for Brain Immunology and Glia, School of Medicine, University of Virginia, Charlottesville, Virginia

<sup>4</sup>Department of Medicine, Duke University, Durham, North Carolina

<sup>5</sup>Department of Pediatrics, Duke University, Durham, North Carolina

<sup>6</sup>Department of Immunology, Duke University, Durham, North Carolina

<sup>7</sup>Department of Pathology, Duke University, Durham, North Carolina

## Correspondence

Anthony J. Filiano, PhD, Marcus Center for Cellular Cures, Departments of Neurosurgery, Immunology, and Pathology, Duke University, 701 W. Main Street, Durham, NC 27701.  
 Email: anthony.filiano@duke.edu

## Funding information

Cord Blood Association; The Marcus Foundation

## Abstract

Mesenchymal stromal cells (MSCs) are widely used in clinical trials because of their ability to modulate inflammation. The success of MSCs has been variable over 25 years, most likely due to an incomplete understanding of their mechanism. After MSCs are injected, they traffic to the lungs and other tissues where they are rapidly cleared. Despite being cleared, MSCs suppress the inflammatory response in the long term. Using human cord tissue-derived MSCs (hCT-MSCs), we demonstrated that hCT-MSCs directly interact and reprogram monocytes and macrophages. After engaging hCT-MSCs, monocytes and macrophages engulfed cytoplasmic components of live hCT-MSCs, then downregulated gene programs for antigen presentation and costimulation, and functionally suppressed the activation of helper T cells. We determined that low-density lipoprotein receptor-related proteins on monocytes and macrophages mediated the engulfment of hCT-MSCs. Since a large amount of cellular information can be packaged in cytoplasmic RNA processing bodies (p-bodies), we generated p-body deficient hCT-MSCs and confirmed that they failed to reprogram monocytes and macrophages in vitro and in vivo. hCT-MSCs suppressed an inflammatory response caused by a nasal lipopolysaccharide challenge. Although both control and p-body deficient hCT-MSCs were engulfed by infiltrating lung monocytes and macrophages, p-body deficient hCT-MSCs failed to suppress inflammation and downregulate MHC-II. Overall, we identified a novel mechanism by which hCT-MSCs indirectly suppressed a T-cell response by directly interacting and reprogramming monocytes and macrophages via p-bodies. The results of this study suggest a novel mechanism for how MSCs can reprogram the inflammatory response and have long-term effects to suppress inflammation.

## KEYWORDS

cell interactions, cellular therapy, immunosuppression, mesenchymal stromal cells, myeloid cells, reprogramming, T cell, umbilical cord

## 1 | INTRODUCTION

Mesenchymal stromal cells (MSCs) are an investigational therapy for a wide range of disorders. They have been extensively used in clinical trials over the past 25 years with variable success.<sup>1</sup> The variability is likely due to the differences in the source tissue and manufacturing procedures to generate MSCs, methods of final preparation and administration, the disease being targeted, and ultimately an unclear understanding of the mechanism of action. Preclinical studies demonstrate a dramatic ability of MSCs to suppress adaptive immunity, thus clinical conditions routinely targeted include a robust T-cell response, such as acute graft-vs-host and autoimmune disease.<sup>2</sup> Although the ability for MSCs to suppress T cells is well documented *in vitro*, little is known how they function *in vivo*.

The ability of MSCs to suppress inflammation relies on complex interactions between many immune cell populations. Some immunomodulatory effects of MSCs could be attributed to release of a spectrum of anti-inflammatory molecules including TGF- $\beta$ ,<sup>3</sup> indoleamine 2,3-dioxygenase (IDO),<sup>4</sup> prostaglandin E<sub>2</sub>,<sup>5</sup> and others. These paracrine signals have well-known immunosuppression capabilities but rely on sustained release. MSCs can induce long-term benefits *in vivo*; however, they are quickly cleared.<sup>6</sup> This suggests that for MSCs to be successful they have a short window to reprogram the inflammatory response.

The majority of intravenously (IV) infused MSCs are transiently detected in the lungs and to a lesser extent in the spleen, liver, kidneys, and lymph nodes where they are surrounded by macrophages.<sup>6</sup> Within hours, IV injected MSCs are rapidly engulfed by monocytes and macrophages to almost undetectable levels 24 hours post infusion. After engulfing MSCs, monocytes and macrophages undergo an anti-inflammatory reprogramming, producing elevated levels of IL-10, IDO, and TGF- $\beta$ .<sup>6,7</sup> If monocytes and macrophages are depleted the ability of MSCs to suppress inflammation is blocked.<sup>8</sup> Although phagocytosis is generally an anti-inflammatory process, there is evidence suggesting a specific response to engulfing MSCs.<sup>6,7</sup> The molecular pathways involved in reprogramming monocytes and macrophages after engulfing MSCs are unknown.

In this study, we demonstrate a novel mechanism of how human umbilical cord tissue derived MSCs (hCT-MSCs) can reprogram monocytes and macrophages. MSC are engulfed by monocytes and macrophages resulting in long-term transcription changes that suppress the activation of T cells. Using computational approaches, we identified potential receptors on monocytes and macrophages that mediated their interactions with hCT-MSC and block the interaction with a pharmacological inhibitor. Furthermore, we identified a key cytoplasmic organelle in hCT-MSCs necessary to reprogram monocytes and macrophages. Our results shed light on how MSCs can modulate the inflammatory response without long-term engraftment.

## 2 | MATERIALS AND METHODS

### 2.1 | Cell culture

hCT-MSCs were obtained from the Robertson GMP lab at Duke. Umbilical cords were drained, cleaned with chlorhexidine gluconate,

### Significance statement

Mesenchymal stromal cells (MSCs) have been used in clinical trials for inflammatory diseases. MSCs are rapidly cleared within hours despite having long-lasting effects in suppressing inflammation. The present study uncovered a novel mechanism by which umbilical cord-derived MSCs reprogram monocytes and macrophages to suppress T cells. Macrophages engulf cytoplasmic components of MSCs and undergo transcriptional reprogramming. The interaction depends on lipoprotein receptor-related proteins on macrophages and is mediated by processing bodies within MSCs. This study not only provides a novel mechanism but also uncovers novel potential therapeutic targets to enhance the immunomodulators capabilities of MSCs.

and separated from the placenta. Under GMP conditions, the cord was cut into small pieces and digested on a gentleMACS Octo Dissociator in buffer containing hyaluronidase, DNase, collagenase, and papain. Cell suspensions were plated on CellBIND 75T flasks (Corning, New York) in Prime-XV MSC Expansion XSFM (FUJIFILM Irvine Scientific, Inc, Santa Ana, California) and incubated in 37°C, 5% CO<sub>2</sub>. Cells were detached using TrypLe Select Enzyme 10X (Thermo Fisher Scientific, Waltham, Massachusetts) and collected for further experiment.

### 2.2 | T-cell proliferation assay

For the proliferation suppression assay, mouse splenocytes were cocultured with hCT-MSCs (1:10 = hCT-MSC:splenocytes) in RPMI 1640 containing 10% FBS, 1% penicillin/streptomycin and 25 mM HEPES with Dynabeads Mouse T-Activator CD3/CD28 (Thermo Fisher Scientific).

For irradiating hCT-MSCs, cells were dosed with 25 Gy, using a cesium irradiator. A total of 33 000 cells were suspended in Prime-XV MSC Expansion XSFM and plated on fibronectin coated 96-well plates then placed in an incubator (37°C, 5% CO<sub>2</sub>). After 48 hours,  $1 \times 10^5$  peripheral blood mononuclear cells (PBMCs) were suspended in RPMI 1640 containing 10% FBS, 1% penicillin/streptomycin and 25 mM HEPES, then plated on hCT-MSCs, and stimulated using Dynabeads human T activator CD3/28 (Thermo Fisher Scientific). After 3 days, 3H thymidine (PerkinElmer, Waltham, MA, USA) was added in each well for a final concentration of 10  $\mu$ Ci/mL and after another 6- to 10-hour incubation, samples were collected using Perkin Elmer Filtermate harvester (PerkinElmer). 3H thymidine incorporation in human PBMCs was measured by a Microbeta Trilux 1450 LSC (PerkinElmer).

For isolating T cells, a Pan T Cell Isolation Kit II (Miltenyi, Bergisch Gladbach, Germany) on a magnetic column was used to select T cells from mouse spleen and lymph nodes. The selected cells were suspended in serum-free RPMI 1640 with 5  $\mu$ M of carboxyfluorescein succinimidyl ester (CFSE; Thermo Fisher Scientific) for 10 minutes

followed by addition of 2× volume of serum-containing media to stop the reaction. The T cells were washed and resuspended in RPMI 1640 containing 10% FBS, 1% penicillin/streptomycin and 25 mM HEPES cocultured with hCT-MSC (1:10 = hCT-MSC:T cells) with Dynabeads Mouse T-Activator CD3/CD28 (Thermo Fisher Scientific). For preconditioning, T cell-depleted splenocytes were prepared using a CD3e microbead kit (Miltenyi) and magnetic separation column, and the cells were preconditioned in a 0.4 μm pore transwell (MilliporeSigma, Burlington, Massachusetts) or directly loaded on plated MSCs (1:10 = hCT-MSC:splenocytes) for 72 hours. Control cells were similarly added to Prime-XV MSC Expansion XFSM for 72 hours. Preconditioned cells were isolated and cocultured with CFSE labeled mouse T cell (1:3 = preconditioned cell:T cells) with Dynabeads Mouse T-Activator CD3/CD28 stimulation. After 72 hours, cells were collected for evaluating proliferation. T cells were treated with Mouse BD Fc Block (BD Bioscience, Franklin Lakes, New Jersey) washed and stained with anti-CD4 APC-H7 (BD Bioscience) antibody and analyzed using a FACSLyric (BD Bioscience) and data were analyzed using BD FACSuite software (BD Bioscience).

Qtracker labeled thymocyte and MSCs were cultured in EdU (Thermo Fisher Scientific) containing media overnight and on the next day, apoptosis was induced by treating thymocytes with 50 μM dexamethasone and hCT-MSCs with 10 μg/mL cycloheximide with 20 ng/mL TNF-α. Cells were washed and cocultured with T cell-depleted splenocyte for 1 day and stained with anti-CD11b and Ly6G. Cells were fixed and incorporated Edu was labeled with Alexa Flour 488. Cells were analyzed using FACSLyric and data were analyzed using BD FACSuite software.

### 2.3 | Phagocytosis assay

Freshly thawed MSCs were labeled with QTracker and EdU according to the manufacturer's instructions then  $2 \times 10^5$  cells were plated on fibronectin coated six-well plates. After 24 hours, the cells were cocultured with T cell-depleted splenocytes for 2 days and splenocytes were collected and stained with anti-B220 PerCPCy5.5, CD11b APC, CD11c Alexa 700, F4/80 PE-Cy7, Ly6C PE, and Ly6G APC-Cy7 (BioLegend, San Diego, California). Cells were analyzed using FACSLyric. For EdU detection, cells were first collected and stained with CD11b APC and after that, cells were fixed, permeabilized and EdU in cells was labeled with Alexa488 according to the manufacturer's instruction. Cells were analyzed using FACSLyric and data were analyzed using BD FACSuite software.

For confocal imaging, hCT-MSCs were labeled with QTracker and plated on fibronectin coated plates for 1 day in RPMI 1640 containing 10% FBS, 1% penicillin/streptomycin and 25 mM HEPES. Then CD11B+ cells were sorted from splenocytes obtained from a C57BL/6-Tg(UBC-GFP)30Scha/J mouse and added to the hCT-MSCs. Images were obtained using Zeiss 780 inverted microscopy.

### 2.4 | RNA sequencing and analysis

QTracker-labeled hCT-MSCs were plated on fibronectin coated six-well plates and after 1 day, splenocytes were added, centrifuged

briefly (1000 rpm, 5 minutes), then cultured for 3 days. Splenocytes were then collected and stained with anti CD11b, Ly6G antibodies. Qtracker positive or negative CD11b<sup>+</sup>Ly6G<sup>-</sup> cells were sorted using a MoFlo Astrios Cell Sorter (Beckman Coulter, Indianapolis, Indiana). RNA from sorted cells was purified by an RNeasy Mini kit (Qiagen, Hilden, Germany) according to manufacturer's instructions. cDNA libraries were generated using KAPA Stranded RNA-Seq Kits (Roche Sequencing Solutions) and sequenced on an Illumina HiSeq 4000. The raw sequencing reads (FASTQ files) were first chastity filtered, which removes any clusters that have a higher than expected intensity of the called base compared to other bases. They were then trimmed with Trimmomatic<sup>9</sup> to remove low-quality bases (minimum read length after trimming, 36). After preprocessing, the quality of the reads was evaluated using FastQC,<sup>10</sup> and after passing quality control, the expression of the transcripts was quantified against the mm10 mouse genome (specifically, the Gencode M13 release)<sup>11</sup> using Salmon.<sup>12</sup> After quantification, the transcript abundances were then imported into R and summarized with tximport (giving gene-level expression estimates),<sup>13</sup> and then DESeq2<sup>14</sup> was used to normalize the raw counts, perform exploratory analysis (eg, principal component analysis), and to perform differential expression analysis. The *P*-values from the differential expression analysis were corrected for multiple hypotheses testing (giving an adjusted *P*-value) with the Benjamini-Hochberg false-discovery rate procedure. Using the differentially expressed genes, the functional terms enriched in the samples was then determined with Fisher's exact test as implemented in the clusterProfiler<sup>15</sup> Bioconductor package. The gene sets used for this analysis were from the Gene Ontology (GO)<sup>16,17</sup> and Kyoto Encyclopedia of Genes and Genomes (KEGG).<sup>18-20</sup>

### 2.5 | Real-time PCR

After coculture with QTracker-labeled hCT-MSCs splenocytes were then collected and stained with anti CD11b, Ly6G antibodies. Qtracker positive or negative CD11b<sup>+</sup>Ly6G<sup>-</sup> cells were sorted using a MoFlo Astrios Cell Sorter. RNA from sorted cells was purified by an RNeasy Mini kit and, then, cDNAs were synthesized using SuperScript VILO cDNA Synthesis Kit (Thermo Fisher Scientific). Real-time PCR was performed on C1000 Touch Thermal Cycler (Bio-Rad) with TaqMan Fast Advanced Master Mix (Applied Biosystems, Foster City, California). The primers (Thermo Fisher Scientific) used in this study were as follows: Ciita, Mm00482914\_m1; H2-DMb2, Mm00783707\_s1; Ox-40L, Mm00437214\_m1; Rfx5, Mm01263513\_g1.

### 2.6 | Phagocytosis inhibitors

For blocker test, hCT-MSCs were labeled using Qtracker and plated on fibronectin-coated 24 well plate. After 1 day, T cell-depleted splenocytes were preincubated for 1 hour in 37°C, 5% CO<sub>2</sub> in each blocker containing culture media in following concentration: Mer RTK

Inhibitor UNC569 (MilliporeSigma): 500 nM; Anti-TREM-2 antibody (MilliporeSigma): 2 µg/mL; Anti-Integrin α9 antibody (MilliporeSigma): 1 µg/mL; GST-receptor-associated protein: 250 nM. After that, cells were collected and resuspended in blocker containing media with the same concentration and then plated on hCT-MSC. Cell plates were briefly centrifuged and incubated for 2 days in 37°C, 5% CO<sub>2</sub>. Cells were collected and stained with anti-CD11b antibody and then analyzed by FACSLyric.

## 2.7 | Mice

Specific pathogen-free C57BL/6 mice were purchased from the Jackson Laboratory. All experiments were performed in accordance with Duke University Institutional Animal Care and Use Committee's policies.

## 2.8 | Generating DDX6 KO hCT-MSCs

DDX6 knockout hCT-MSCs were manufactured in the Duke Functional Genomics Shared Resource Core. To generate DDX6 knock out cell using CRISPR/Cas9 technology, sgRNA targeting DDX6 exon 3 was cloned into Cas9 expressing AAV vector. The following oligonucleotides from sense strand were used for sgRNAs targeting DDX6 exon 3: TCTCTAGACCTGGTGATGAC. For control hCT-MSCs, a nontargeting gRNA sequence was used: ATACTCTGATCTCACTCATTT. For viral transduction, hCT-MSC were incubated with AAVS1 containing culture supernatant and after 3 days, cells were treated with puromycin over 2 days for virally transduced cell selection. Media was changed and cells were cultured for further experiments. All work using recombinant DNA was approved and followed NIH guidelines.

## 2.9 | DCP1A expression in hCT-MSC

For transfecting hCT-MSCs, cells were plated on fibronectin coated 24-well plates, and incubated in normal cell incubation condition (37°C, 5% CO<sub>2</sub>) for 2 days until the cells reached ~80% confluency. For transient expression of DCP1A or DDX6, 1 µg of DCP1A-GFP plasmid was mixed with Lipofectamine 3000 (Thermo Fisher Scientific) according to manufacturer instruction or DDX6-RFP plasmid was mixed with TransIT-2020 transfection reagent (Mirus Bio LLC) at the ratio of reagent:DNA at 3:1 and DNA-reagent mixture was added on hCT-MSC. After 48 hours, the media was changed with Prime-XV MSC Expansion XFSM. To determine if p-bodies were transferred to monocytes or macrophages, transfected hCT-MSCs were incubated with CD11b+ MAC sorted monocytes and macrophages isolated from UBC-GFP mouse spleens for 4 hours. GFP+ monocytes and macrophages were then transferred to a new plate for imaging. DCP1A-GFP or DDX6-RFP punta in hCT-MSC or monocytes and macrophage were detected using Leica SP8 upright confocal microscopy (Leica Microsystems).

## 2.10 | Western blot

Control or DDX6 KO hCT-MSC were lysed in protease inhibitor (MilliporeSigma) containing RIPA lysis buffer (MilliporeSigma) and separated using SDS polyacrylamide gel. The protein was transferred to PVDF membrane and blocked with 5% skim milk in PBS containing 0.05% Tween 20 and blotted using anti-DDX6 and β-actin antibodies (Abcam, Cambridge, UK). Subsequently, the blots were developed using the ECL Detection Kit (Bio-Rad Laboratories, Hercules, California) and protein bands were visualized using C-digit blot scanner (LI-COR Biosciences, Lincoln, Nebraska).

## 2.11 | Immunohistochemistry

hCT-MSCs were plated on fibronectin coated cover slides and incubated for 2 days. After, cells were fixed using 4% paraformaldehyde and incubated with blocking buffer (5% normal goat serum, 2% BSA, and 0.1% Triton X-100 in PBS) and stained using anti-DDX6 (abcam) and anti-Dcp1a antibody (Santa Cruz Biotechnology, Inc, Dallas, Texas). The cells were incubated with Alexa 488-conjugated secondary antibodies and mounted with VectaShield medium (Vector Labs, Burlingame, California). The images were acquired using Leica SP8 upright confocal microscopy (Leica Microsystems, Inc, Wetzlar, Germany). Z-stacks were analyzed by ImageJ for orthogonal views or Imaris Bitplane software 9.1.2 for 3D reconstruction.

## 2.12 | Lipopolysaccharide-induced lung inflammation

Eight-week-old mice received vehicle, control hCT-MSC, or DDX6 KO hCT-MSC ( $2 \times 10^6$  cells/150 µL) through IV injection 2 hours prior to lipopolysaccharide (LPS; 10 µg/50 µL) intranasal administration. Twenty-four hours after LPS administration, mice were sacrificed and lungs were collected for further analysis. Lungs were dissected into small pieces and enzymatically digested with liberase (0.2 mg/mL; MilliporeSigma) and DNase I (0.1 mg/mL) at 37°C for 30 minutes in serum free RPMI and filtered by 70 µ cell strainer. The cells were treated with Mouse BD Fc Block and then stained by anti-CD3, CD11b, CD11c, Siglec F, I-A/I-E (biolegend), and 7AAD. Cells were analyzed using FACSLyric and data were analyzed using the BD FACSuite software.

## 2.13 | Statistics

Statistical analysis using a one-way ANOVA followed by a Bonferroni post hoc analysis was performed using the Prism software (GraphPad Software Inc, La Jolla, California) unless otherwise described in the figure legends.

### 3 | RESULTS

#### 3.1 | hCT-MSCs suppress T-cell activation via programming myeloid cell

We cultured hCT-MSCs isolated from umbilical cord tissue and confirmed they express canonical MSC markers by flow cytometry (Figure S1A) and have the potential to differentiate to adipocytes,

osteocytes and chondrocytes (Figure S1B). hCT-MSCs were not contaminated by endothelial cells (CD31<sup>+</sup>) or hematopoietic cells (CD45<sup>+</sup>; Figure S1). To test if hCT-MSCs can inhibit a T-cell response, we cocultured them with human peripheral blood mononuclear cells (PBMCs) stimulated with anti-CD3/28 antibodies. hCT-MSCs inhibited T-cell proliferation (Figure 1A) and suppressed the expression of activation markers CD25 and CD69 on helper T cells (T<sub>H</sub>; Figure S2A-C). hCT-MSC also suppressed T<sub>H</sub> cell activation in

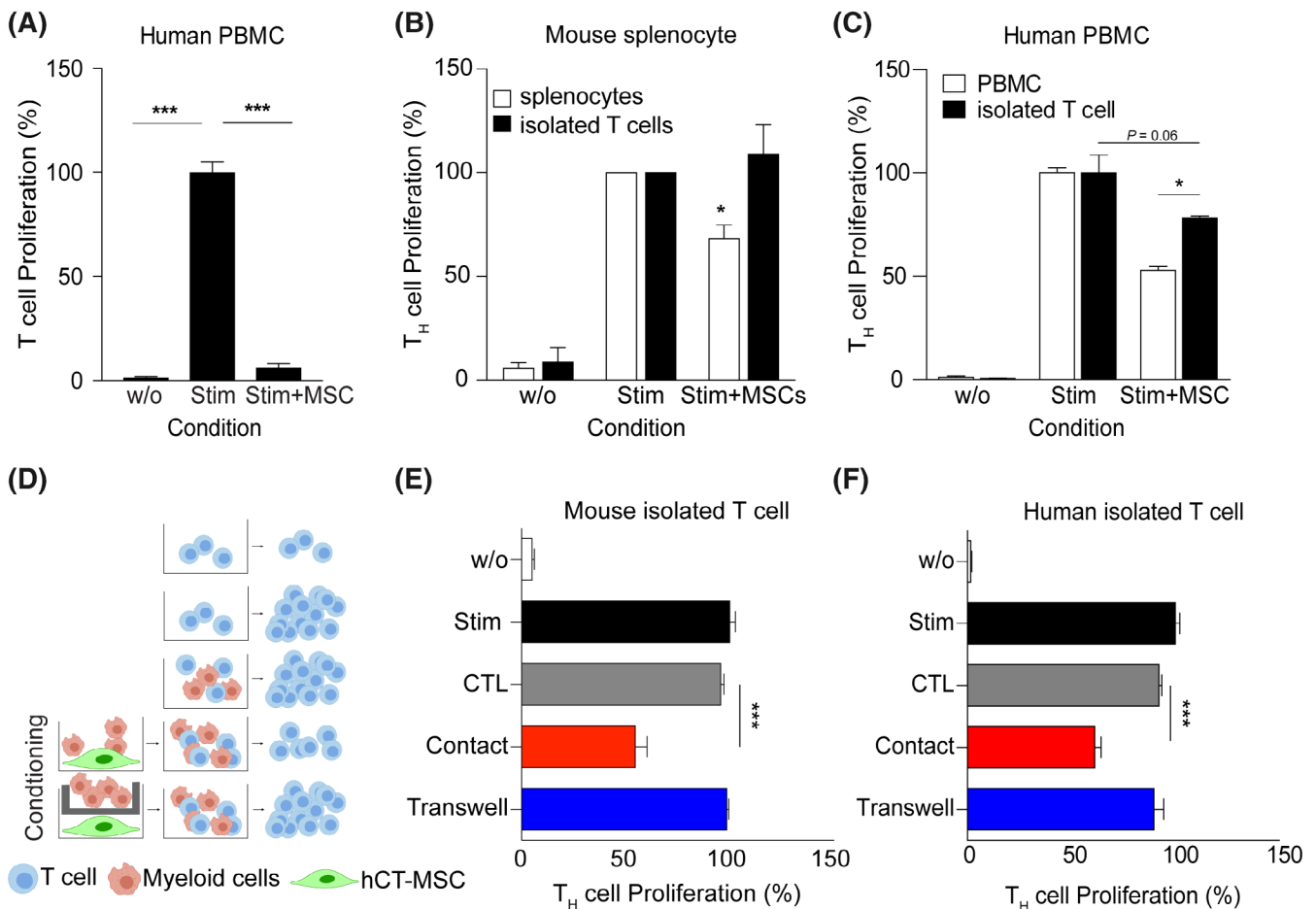


**FIGURE 1** hCT-MSCs program monocytes and macrophages to inhibit the activation of T cells. A, hCT-MSCs inhibit the proliferation of T cells from human PBMCs. T-cell proliferation was measured in counts/minute by the incorporation of 3H-thymidine (one-way ANOVA; post hoc  $***P < .001$ ; N = 3). B, T<sub>H</sub> cell proliferation assay. T cells were stained with CFSE and proliferation of CD4<sup>+</sup> T<sub>H</sub> cells was measured by CFSE dilution after stimulated with anti-CD3/28. hCT-MSCs block T<sub>H</sub> cell proliferation in a population of splenocytes (open bars) but not isolated T cells (black bars; two-way ANOVA; post hoc  $*P < .05$ ). C, Whole human PBMC or T cells from human PBMC were stained with CFSE and cocultured with hCT-MSC with anti-CD3/28. After 3 days after, cells were stained using anti-CD4 and T<sub>H</sub> cell proliferation was measured by CFSE dilution (black bars; two-way ANOVA; post hoc  $*P < .05$ ). D, Experimental schematic for programming monocytes and macrophages. E, hCT-MSCs physically interact with mouse monocytes and macrophages, then monocytes and macrophages can suppress T cells when transferred to a new well (red bar). Conversely, if monocytes and macrophages were cultured in MSC expansion media without being exposed to hCT-MSCs (CTL gray bar) or are blocked from directly interacting with hCT-MSCs, via a transwell membrane (blue bar), they no longer suppress T cells (one-way ANOVA; post hoc  $***P < .001$ ). F, T cell-depleted human PBMCs were preconditioned by hCT-MSC coculture in same well (red bar) or in the transwell to block direct cell-to-cell contact (blue bar). Control (CTL; gray bar) T cell-depleted PBMCs were incubated in MSC expansion media without hCT-MSCs. Preconditioned cells were transferred to CFSE labeled isolated human T cell with anti-CD3/28 and proliferation of T<sub>H</sub> cell were measured by CFSE dilution (one-way ANOVA; post hoc  $***P < .001$ ; N = 3). CFSE, carboxyfluorescein succinimidyl ester; hCT-MSC, human umbilical cord tissue mesenchymal stromal cell; PBMC, peripheral blood mononuclear cell

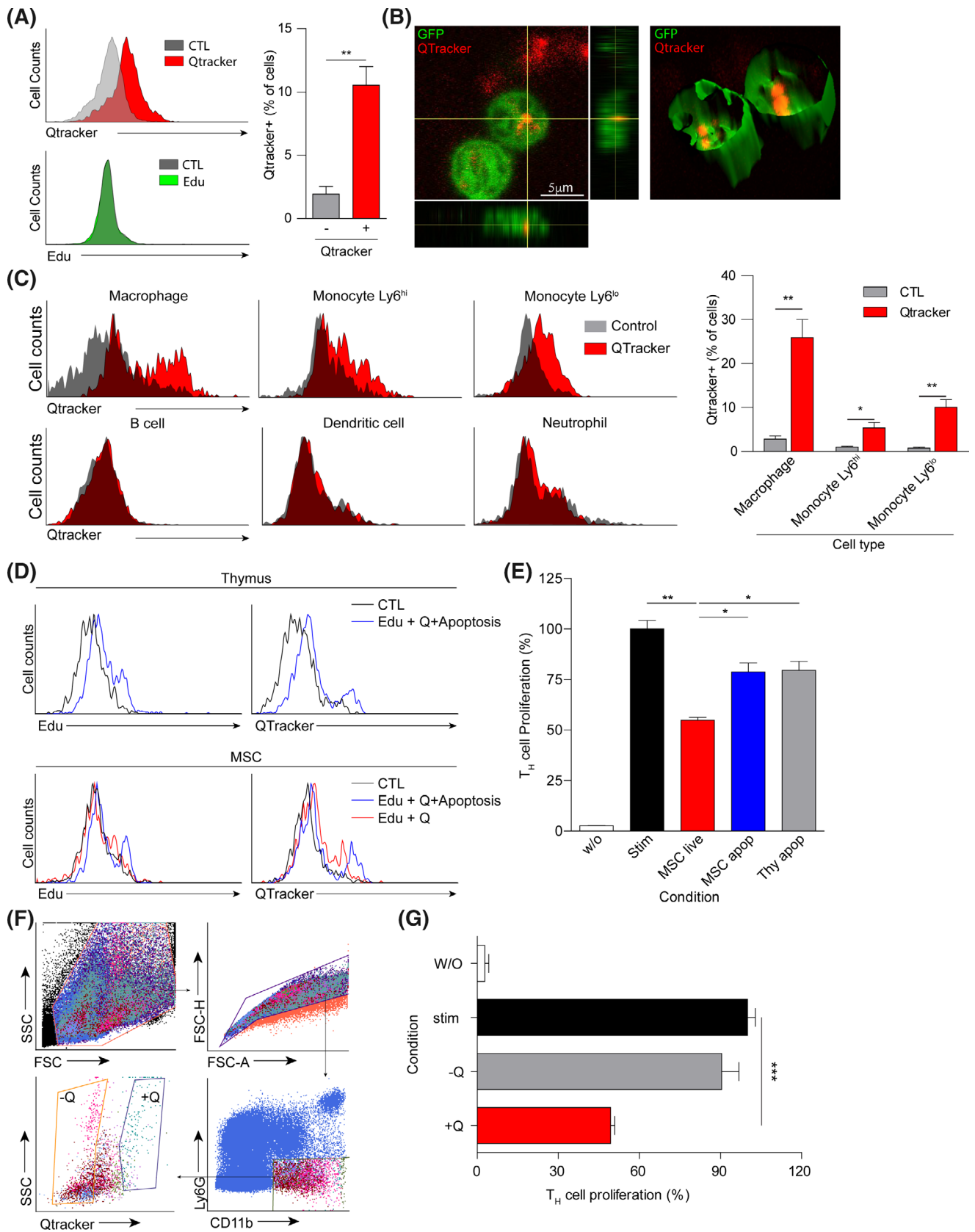


**FIGURE 2** Legend on next page.

mouse splenocytes. Interestingly, although hCT-MSCs inhibited T<sub>H</sub> cells within a bulk splenocyte pool, hCT-MSCs failed to inhibit the proliferation of isolated T<sub>H</sub> cells suggesting that a non-T cell is needed for the immune suppression function of hCT-MSCs (Figure 1B). Similar results were found in human blood where hCT-MSCs suppressed T<sub>H</sub> cells in PBMCs to a much greater extent than isolated T<sub>H</sub> cells (Figure 1C). Immunosuppression was specific to hCT-MSCs since human umbilical vein endothelial cells (HUVECs) did not affect the proliferation of T<sub>H</sub> cells (Figure S2D). Since *in vivo* data demonstrate that MSCs can have long-lasting beneficial effects despite being quickly cleared, and MSC-primed monocytes can induce regulatory T-cell populations,<sup>6</sup> we hypothesized that MSCs must interact with myeloid cells to successfully inhibit T cells. To test this, we preconditioned mouse splenocytes or human PBMC, depleted of T cells, with hCT-MSCs prior to coculturing with activated T cells (Figure 1D). Both mouse splenocytes and human PBMC, depleted of T cells and preconditioned with hCT-MSC, inhibited T<sub>H</sub> cell proliferation in the absence of hCT-MSCs (Figure 1E,F). We confirmed that hCT-MSCs did not transfer over to the T-cell proliferation assay (Figure S3A) and the ability for preconditioned cells to suppress T<sub>H</sub> cells was retained for at least 48 hours (Figure S2E). In order to be preconditioned, myeloid populations must physically interact with the hCT-MSCs since the effect was abolished if the cells were separated by a transwell filter (Figure 1D,E,F). These data suggest that direct cell-to-cell contact is critical for hCT-MSCs to reprogram myeloid populations.

### 3.2 | Engulfment of hCT-MSCs is critical to reprogramming monocytes and macrophages

MSCs injected intravenously in mice are rapidly cleared within 24 hours. Because their remnants can be detected in CD11b<sup>+</sup> myeloid cells,<sup>6,7</sup> we hypothesized CD11b<sup>+</sup> myeloid cells with direct cell-to-cell contact would engulf hCT-MSCs in our assay. To address this, we labeled the cytoplasm of hCT-MSCs with Qtracker and the nucleus with Edu, then tested the ability of splenic myeloid cells to engulf live

hCT-MSCs. Like others, we detected CD11b<sup>+</sup>/Qtracker<sup>+</sup> myeloid cells 2 days after being incubated with labeled hCT-MSCs (Figure 2A,B). However, we did not detect Edu in any splenocytes (Figure 2A). Since Edu is incorporated into DNA during replication while Qtracker is restricted to the cytosol, we concluded that myeloid cells only engulf cytosolic components of live hCT-MSCs but do not phagocytose the entire cell. Furthermore, we identified that the cells which uptake hCT-MSCs were mostly macrophages and Ly6C<sup>lo</sup> resident monocytes, with a smaller percent of Ly6C<sup>hi</sup> inflammatory monocytes positive for Qtracker (Figure 2C; Figure S4). Phagocytosis of apoptotic cells (ie, efferocytosis) can skew professional phagocytes to an anti-inflammatory phenotype. Therefore, we tested if monocytes and macrophages incubated with apoptotic hCT-MSCs or apoptotic thymocytes would also inhibit the activation of T<sub>H</sub> cells. Unlike when incubated with live hCT-MSCs, monocytes and macrophages phagocytosed whole apoptotic hCT-MSCs and thymocytes, as expected, indicated by Edu positive signal in macrophages (Figure 2D; Figure S5). In agreement with other studies, efferocytosis of either type of apoptotic cells resulted in monocytes and macrophages suppressing the proliferation of T<sub>H</sub> cells; however, neither suppressed to the same extent as macrophages that engulfed cytoplasmic components of live hCT-MSCs (Figure 2E). To test if engulfing cytoplasmic components of hCT-MSCs is a critical process to reprogramming monocytes and macrophages, we isolated Qtracker positive or negative monocytes and macrophages by fluorescence-activated cell sorting (FACS) after they were cocultured with live labeled hCT-MSCs (Figure 2F). Qtracker<sup>+</sup> monocytes and macrophages inhibited T<sub>H</sub> cell proliferation while Qtracker<sup>-</sup> cells failed to inhibit T-cell proliferation (Figure 2G).

### 3.3 | Transcriptional and functional alterations in monocytes and macrophages after engulfing components of hCT-MSCs

To understand functional changes monocytes and macrophages undergo after engulfing components of live hCT-MSCs, we FACS

**FIGURE 2** Monocytes and macrophages that engulf hCT-MSCs are programmed to inhibit T cells. A, hCT-MSCs were labeled with Qtracker (cytoplasmic stain) or Edu (nuclei stain) then incubated with macrophages. Monocytes and macrophages take up Qtracker but not Edu. Qtracker and Edu signal were analyzed by flow cytometry (representative histograms) and the percent of monocytes and macrophages that are Qtracker positive were quantified (*t* test  $**P < .01$ ; *N* = 3). B, Representative confocal z-stacks and 3D reconstruction of hCT-MSCs labeled with Qtracker and cocultured with GFP<sup>+</sup> monocytes and macrophages. C, T cell-depleted splenocytes were cocultured with Qtracker labeled hCT-MSCs and 2 days afterwards, cells were stained with anti-B220, CD11b, CD11c, F4/80, Ly6C, Ly6G to analyze the cell type which engulfed hCT-MSCs (Macrophage: CD11b<sup>+</sup>F4/80<sup>+</sup>Ly6G<sup>-</sup>; Monocyte Ly6C<sup>hi</sup>: CD11b<sup>+</sup>F4/80<sup>-</sup>Ly6G<sup>-</sup> Ly6C<sup>hi</sup>; Monocyte Ly6C<sup>lo</sup>: CD11b<sup>+</sup>F4/80<sup>-</sup>Ly6G<sup>-</sup> Ly6C<sup>lo</sup>; B cell: CD11b<sup>-</sup>B220<sup>+</sup> Dendritic Cell: CD11b<sup>-</sup>CD11c; Neutrophil: CD11b<sup>+</sup>Ly6G<sup>+</sup>; [*t* test  $*P < .05$ ,  $**P < .01$ ; *N* = 3]). D, Representative histograms of CD11b<sup>+</sup>Ly6G<sup>-</sup> cells after incubating with Qtracker/Edu labeled cells (live or apoptotic hCT-MSCs and thymocytes). E, T-cell proliferation assay. CD11b<sup>+</sup> cells were isolated from collected splenocytes and cocultured with CFSE-labeled T cell with anti-CD3/28 stimulation for 3 days. CFSE signal of T cells was measured using BD FACSLytic (one-way ANOVA; post hoc  $*P < .05$ ,  $**P < .01$ ; *N* = 3). F, T cell-depleted splenocytes were cocultured with Qtracker labeled MSC for 2 days and stained using anti-CD11b and Ly6G. Qtracker positive/negative CD11b<sup>+</sup>, Ly6G<sup>-</sup> cells were sorted using MoFlo Astrios Cell Sorter. G, Monocytes and macrophages were FACS sorted on their ability to engulf hCT-MSCs (ie, Qtracker positive and negative), then tested for their ability to inhibit T cells. T-cell proliferation was measured by CFSE dilution (one-way ANOVA; post hoc  $***P < .001$ ; *N* = 3). CFSE, carboxyfluorescein succinimidyl ester; FACS, fluorescence-activated cell sorting; hCT-MSC, human umbilical cord tissue mesenchymal stromal cell

sorted and sequenced RNA of Qtracker positive or negative monocytes and macrophages 48 hours after coculture with hCT-MSCs. Principal component analysis of statistically significant transcripts revealed that the two populations were transcriptionally distinct (Figure 3A).

To understand functional differences of these populations, we performed a gene set enrichment analysis and determined that the top gene sets downregulated in Qtracker positive monocytes and macrophages were associated with the activation of T cells, in particular genes associated with antigen presentation, while upregulated

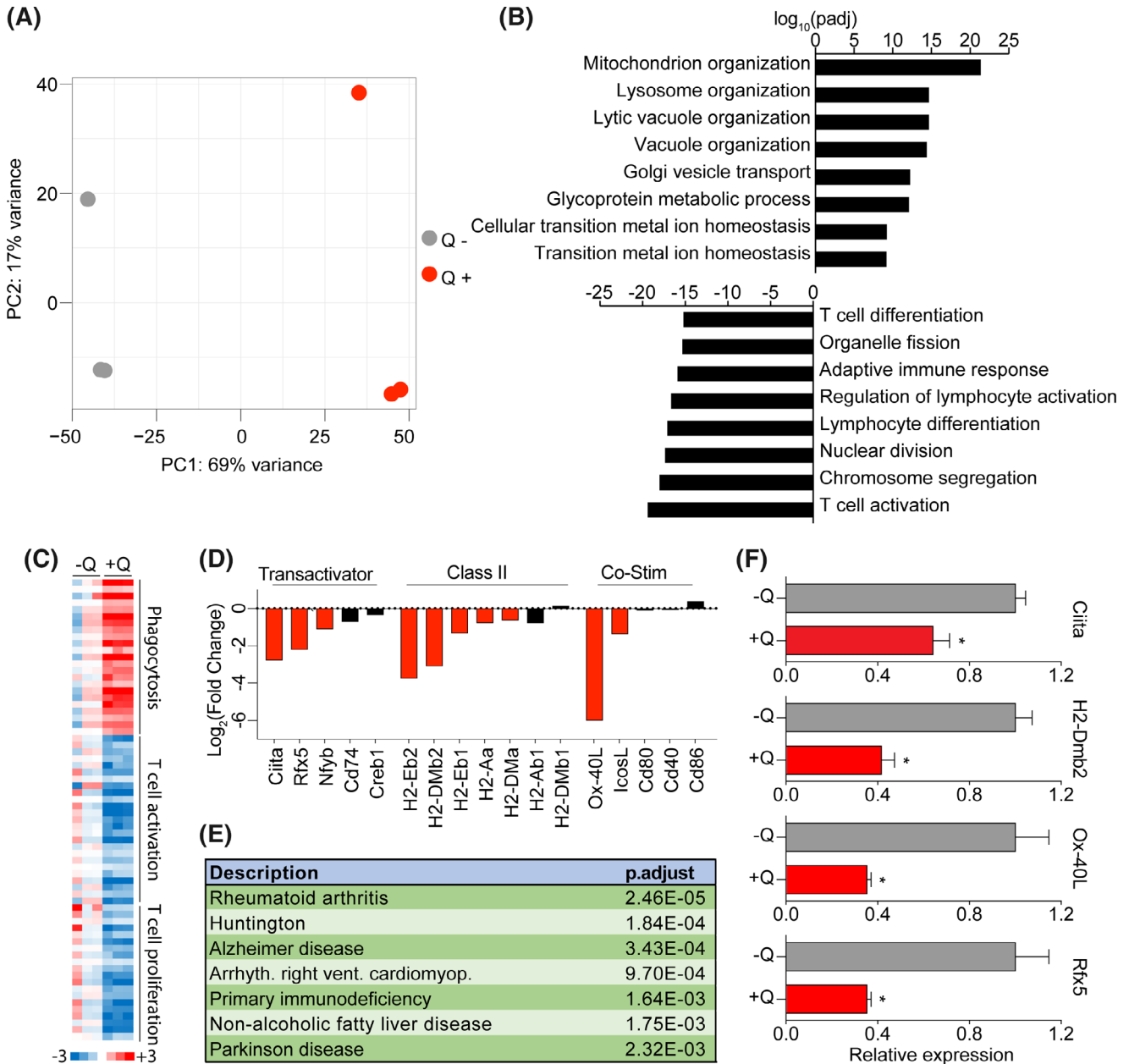


**FIGURE 3** Transcriptional changes of monocytes and macrophages after engulfing cytoplasmic components of human umbilical cord tissue mesenchymal stromal cell (hCT-MSCs). A-E, After 2-day coculture with Qtracker labeled hCT-MSC, mouse splenocytes were collected and Qtracker positive/negative CD11b+, Ly6G- cells were sorted using MoFlo Astrios Cell Sorter. RNAs were collected from each cells for RNA sequencing. A, PCA analysis of Q+ and Q- monocytes and macrophages. B, Gene sets enriched in Qtracker positive (Q+) and Qtracker negative (Q-) monocytes and macrophages. C, Qtracker positive monocytes and macrophages upregulate genes associated with phagocytosis and downregulated genes associated with T-cell activation or proliferation. D, Qtracker positive monocytes and macrophages downregulated associated with antigen presentation and costimulation. E, Genes related with diseases differentially expressed in Qtracker positive monocytes and macrophages. F, Expression of mRNAs related with antigen presentation were decreased in Q+ monocytes and macrophages

gene sets were associated with cellular organization (Figure 3B-F). The mostly highly enriched disease sets included rheumatoid arthritis and primary immunodeficiency (Figure 3E). With these data, we conclude that monocytes and macrophages that engulf cytoplasmic components of hCT-MSC are transcription poised to inhibit the activation of T<sub>H</sub> cells.

Phagocytosis and other cell engulfment pathways are mediated by ligand-receptor interactions. To determine a potential receptor on monocytes and macrophages needed to engulf cytoplasmic components of MSCs, we curated molecules involved in cell-to-cell interactions<sup>21,22</sup> and plotted the gene expression of these molecules upregulated in Qtracker<sup>+</sup> monocytes and macrophages (Figure 4A). We were able to identify pharmacological inhibitors for six of the seven top hits: low-density lipoprotein receptor-related proteins (LRP1, 11, and 12), MER proto-oncogene, tyrosine kinase (MERTK), integrin subunit alpha 9 (ITGA9), and triggering receptor expressed on myeloid cells 2 (TREM2). Only receptor associated protein (RAP<sup>23</sup>), a pan inhibitor of LRPs was able to inhibit monocytes and macrophages from engulfing cytoplasmic components of hCT-MSC (Figure 4B,C; Figure S6). These data suggest that the interaction between monocytes and macrophages and hCT-MSCs is mediated through LRPs and results in monocytes and macrophages engulfing cytoplasmic components of hCT-MSCs.

### 3.4 | Process body-dependent reprogramming of macrophages

Given that monocytes and macrophages must engulf cytoplasmic components to suppress T<sub>H</sub> cells, we explored potential mechanisms

how cells could package and transfer large amounts of information via cytoplasm. Processing bodies (p-bodies) are cytosolic membrane-less organelles that store RNA, miRNA, and proteins. Using antibodies detecting DCP1A (decapping mRNA 1A) or DDX6 (DEAD-Box Helicase), major components of p-bodies, we found that p-bodies are abundant in hCT-MSCs (Figure 5A). We hypothesized that p-bodies in hCT-MSCs function to store packaged information to be transferred to functionally reprogram monocytes and macrophages. To address this, we first tested if p-bodies from hCT-MSC are transferred to monocytes and macrophages. After coculturing monocytes and macrophages with hCT-MSC that transiently overexpressed DDX6-RFP, we were able to detect DDX6-RFP signal in the monocytes and macrophages (Figure 5B,C). These data suggest that p-bodies in hCT-MSC can be transferred to monocytes and macrophages. Next, we generated DDX6 knockout hCT-MSC cells with CRISPR/Cas9 (Figure 5D). DDX6 is an RNA binding protein critical to stabilize p-bodies.<sup>24</sup> As expected, DDX6 knockout hCT-MSCs failed to produce p-bodies (Figure 5E). Although monocytes and macrophages could still engulf components of DDX6-knockout hCT-MSCs (Figure S7A), they failed to program monocytes and macrophages and suppress the proliferation of human and mouse T<sub>H</sub> cells (Figure 5F-H). To note, we did not detect changes in viability of DDX6 knockout hCT-MSCs (Figure S7B). We conclude that p-bodies within hCT-MSCs are a critical component to reprogramming monocytes and macrophages to inhibit the activation of T<sub>H</sub> cells.

p-Bodies in hCT-MSCs are critical to suppress inflammation in the lung. To test the function of hCT-MSC p-bodies in vivo, we induced lung inflammation with intranasal LPS. Two hours before administering LPS, we injected (IV) control hCT-MSCs or DDX6 KO hCT-MSCs. To track hCT-MSCs, we labeled the cells with QTracker.

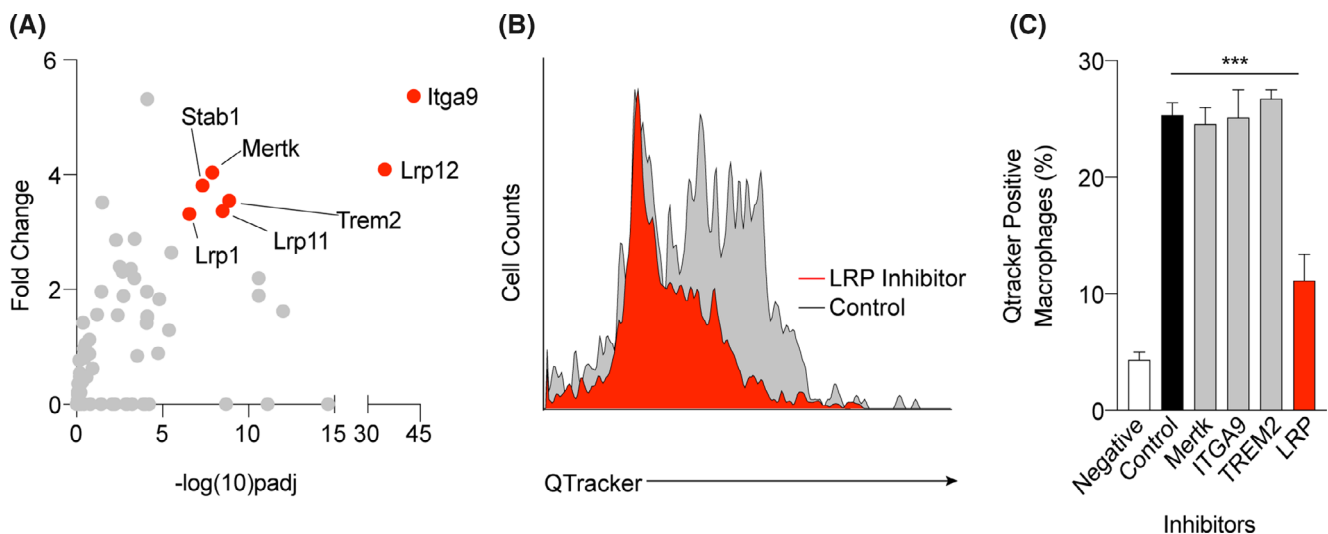


**FIGURE 4** Monocytes and macrophages interact with MSCs through LRP. A, Genes that express receptors mediating cell-to-cell interactions were curated and plotted for differential expression upregulated in monocytes and macrophages that engulf cytoplasmic components of MSCs. The top seven upregulated and lowest adjusted *P*-values are marked in red. Inhibitors for six of seven receptors were tested in our Qtracker MSC engulfment assay, including RAP, a pan inhibitor of LRPs. B, Representative histogram of Qtracker positive macrophages (*N* = 3). C, Quantification of the percent of monocytes and macrophages that are Qtracker positive (one-way ANOVA; post hoc \*\*\**P* < .001; *N* = 3). LRP, low-density lipoprotein receptor-related proteins; MSC, mesenchymal stromal cell; RAP, receptor associated protein

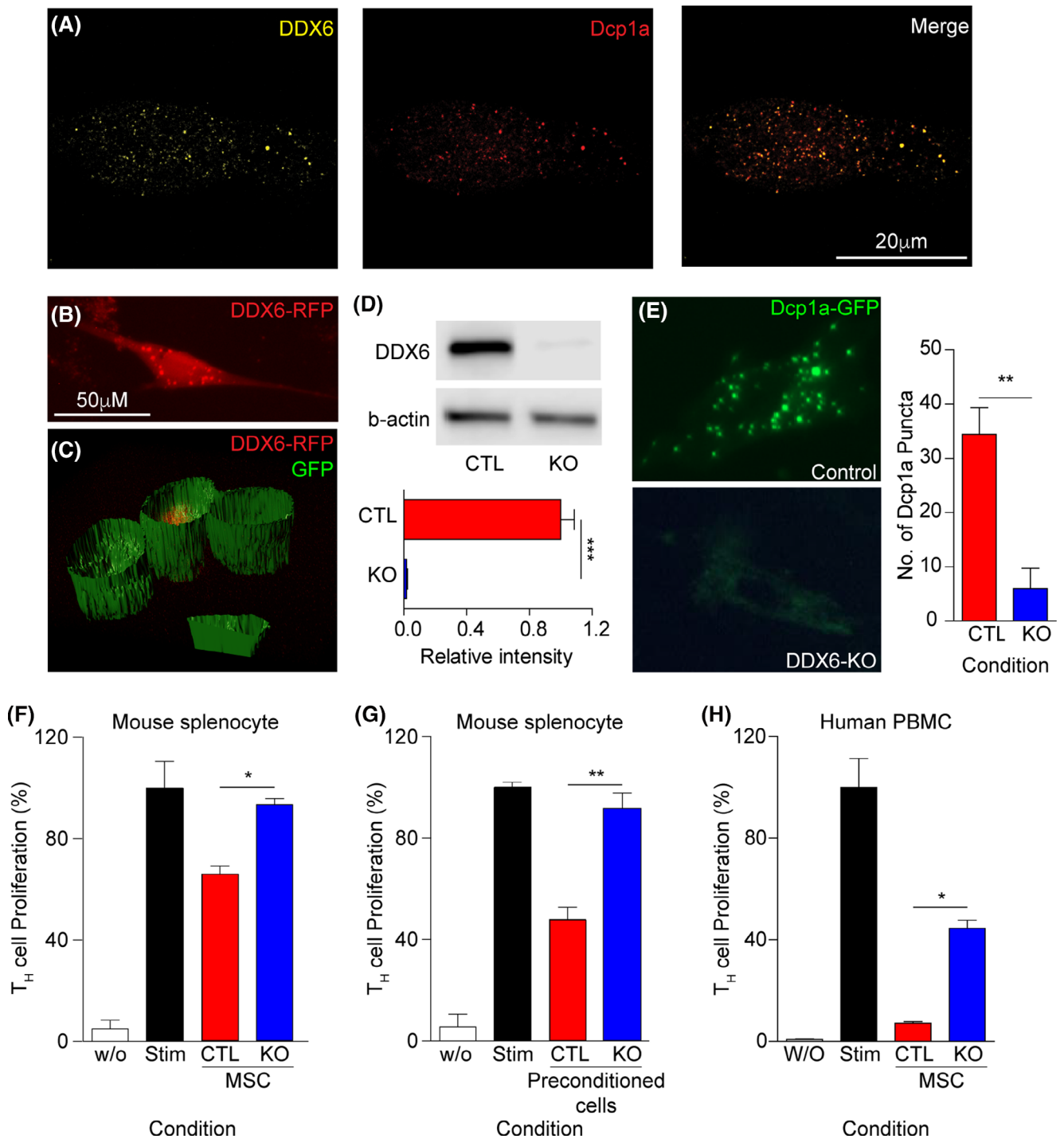


**FIGURE 5** p-Bodies are needed to program macrophages to inhibit T<sub>H</sub> cell activation. A, Representative confocal image of hCT-MSCs stained with DCP1A and DDX6 antibodies. B, Representative image of hCT-MSC transiently transfected with DDX6-RFP obtained by confocal. C, 3D reconstruction of monocytes or macrophages which engulfed DDX6-RFP from hCT-MSC. D, Western blot analysis was performed to detect DDX6 protein expression in control hCT-MSCs and DDX6 KO hCT-MSCs (t test \*\*\*P < .001; N = 3). E, Representative confocal image and Dcp1a puncta counts of control and DDX6-KO hCT-MSCs transiently transfected with DCP1a-GFP (N = 5). F, CFSE labeled mouse splenocytes were cocultured with control or DDX6 KO MSCs and stimulated with anti-CD3/28 (one-way ANOVA; post hoc \*P < .05; N = 3). G, T cell-depleted mouse splenocytes were preconditioned by control or DDX6 KO MSC for 3 days. Then, preconditioned cells were transferred to CFSE-labeled T cell stimulated with anti-CD3/28 (one-way ANOVA; post hoc \*\*P < .01; N = 3). H, Whole human PBMC were stained with CFSE and cocultured with control or DDX6 KO hCT-MSCs then stimulated with anti-CD3/28. After 3 days, cells were stained using anti-CD4 and T<sub>H</sub> cell proliferation was measured by the incorporation of 3H-thymidine (one-way ANOVA; post hoc \*P < .05; N = 3). hCT-MSC, human umbilical cord tissue mesenchymal stromal cell; CFSE, carboxyfluorescein succinimidyl ester; PBMC, peripheral blood mononuclear cell

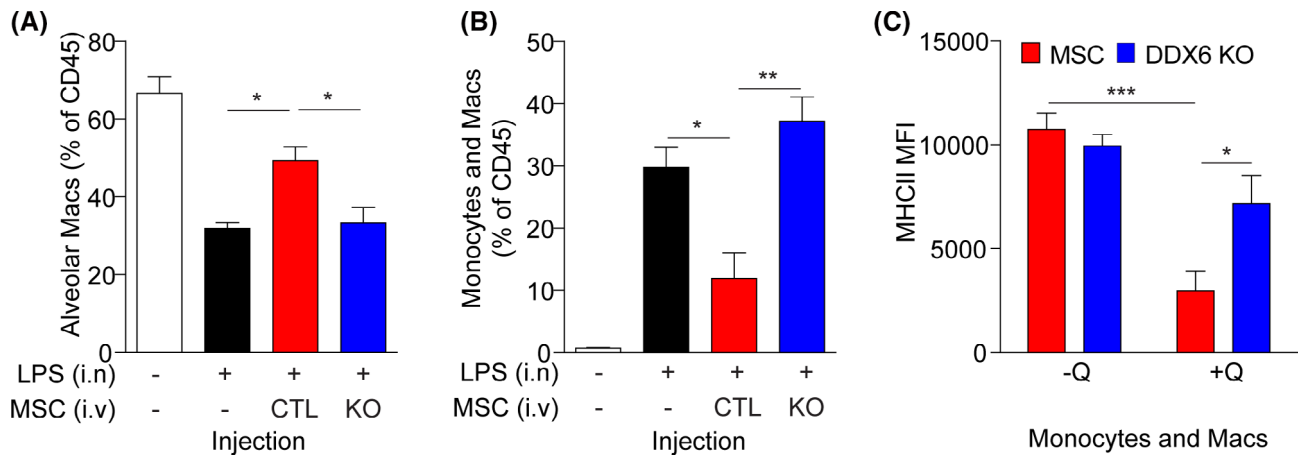


**FIGURE 6** p-Bodies are needed to suppress monocytes and macrophages during lung inflammation. Control or DDX6 KO hCT-MSCs were injected IV 2 hours prior to mice receiving intranasal LPS to induce lung inflammation. Cells were isolated from lung and stained with anti-CD3, CD11b, CD11c, I-A/I-E, and 7AAD then analyzed by flow cytometry. A, CD11b<sup>-</sup>/CD11c<sup>+</sup>/Siglec-F<sup>+</sup> Alveolar macrophage populations from lungs (one-way ANOVA; post hoc \**P* < .05; *N* = 3-4). B, CD11b<sup>+</sup> infiltrating monocytes and macrophage populations from lungs (one-way ANOVA; post hoc \**P* < .05; \*\**P* < .01; *N* = 3-4). C, MHC class II expression on lung CD11b<sup>+</sup>/CD11c<sup>-</sup> infiltrating monocytes and macrophages were measured by FACS flow (one-way ANOVA; post hoc \**P* < .05; \*\*\**P* < .001; *N* = 3-4). hCT-MSC, human umbilical cord tissue mesenchymal stromal cell; LSP, lipopolysaccharide; MSC, mesenchymal stromal cell; FACS, fluorescence-activated cell sorting

Twenty-four hours after LPS, we detected Qtracker signal within infiltrating lung monocytes and macrophages, suggesting they engulfed hCT-MSCs (Figure S8B). Importantly, DDX6 KO hCT-MSCs were engulfed to the same extent as control hCT-MSCs. Functionally, hCT-MSCs blocked an LPS-induced loss of CD11c<sup>+</sup> alveolar macrophages (Figure 6A) and an increase in CD11b<sup>+</sup> inflammatory monocytes and macrophages populations in lung tissue (Figure 6B). Importantly, CD11b<sup>+</sup> infiltrating monocytes and macrophages that engulfed components of hCT-MSC had decreased surface expression of MHC-II (Figure 6C). Compared to control hCT-MSCs, DDX6 KO hCT-MSCs failed to block a loss of alveolar macrophages or an influx in inflammatory CD11b<sup>+</sup> cells in the lung (Figure 6A,B). Furthermore, MHC-II expression on CD11b<sup>+</sup> infiltrating monocytes and macrophages which engulfed DDX6 KO hCT-MSCs was not altered (Figure 6C). These data demonstrate that p-bodies in hCT-MSC are critical component for suppressing inflammation.

## 4 | DISCUSSION

MSCs represent approximately 25% of all cell-based clinical trials with over 1000 trials registered on ClinicalTrials.gov.<sup>25</sup> MSCs are well documented to influence multiple immune cell populations yet how they confer benefit in vivo is unclear. Despite demonstrating long-lasting effects in vivo, MSCs do not engraft and are rapidly cleared. This enigma defines a critical barrier advancing MSCs as a reliable therapeutic option for inflammatory disease.

Our data demonstrate that hCT-MSCs indirectly suppress the activation of T<sub>H</sub> cells through interacting with monocytes and macrophages. This corroborates other findings demonstrating that monocytes and macrophages are necessary for the beneficial effects of MSCs in vitro.<sup>26-28</sup> Likewise, the interactions in vivo between MSCs

and monocytes and macrophages are critical to suppress a pro-inflammatory adaptive immune response. In a mouse model of graft-vs-host disease, MSCs prevented effector T cells from infiltrating the lungs and spleen.<sup>7</sup> Labeled MSCs homed to the lungs and were engulfed by monocytes and macrophages. Similarly, in mouse models of sepsis, labeled MSCs are engulfed by alveolar macrophages and increase survival.<sup>28,29</sup> In both models, depleting macrophages with clodronate-filled liposomes blocked any beneficial effects of MSCs. It is presumed that once injected, MSCs undergo apoptosis then macrophages phagocytose the labeled MSC corpses (efferocytosis); however, we determined an alternate mechanism where monocytes and macrophages instead engulf cytoplasmic components of live MSCs (Figure 2).

In our assays (Figure 1C) and others, the ability of MSCs to reprogram monocytes and macrophages was dependent on direct contact.<sup>27,28</sup> When monocytes and macrophages were separated from hCT-MSCs by a transwell membrane, they failed to suppress activated T<sub>H</sub> cells. The pore size (0.4 μM) in the transwells would not prevent the passage of exosomes (30-100 nm), suggesting reprogramming depended on direct cellular contact. When we colabeled hCT-MSC with Qtracker to label the cytoplasm and EdU to label the nucleus, we found that monocytes and macrophages only took up Qtracker (Figure 2A). Consequently, only cells that took up Qtracker from hCT-MSCs were reprogrammed to suppress T<sub>H</sub> cells (Figure 2G). When we induced apoptosis of Qtracker<sup>+</sup>/EdU colabeled hCT-MSCs, then monocytes and macrophages phagocytosed entire hCT-MSCs (ie, cells took up Qtracker and EdU; Figure 2D). Monocytes and macrophages, after efferocytosis of hCT-MSCs, attenuated T cell proliferation; however, the response was not as robust as after engulfing cytoplasmic components of live hCT-MSCs (Figure 2E). Furthermore, monocytes and macrophages attenuated T<sub>H</sub> cell proliferation to similar level after efferocytosis of apoptotic

thymocytes. These data suggest two separate mechanisms driving anti-inflammatory responses in professional phagocytes (a) a non-specific anti-inflammatory response from efferocytosis and (b) a specific response that depends on contact-mediated transfer of cytoplasmic components of live hCT-MSCs.

Although efferocytosis likely contributes to engulfing and clearing MSCs; trogocytosis (nibbling),<sup>30,31</sup> paracytophagy,<sup>32</sup> and tunneling nanotubes<sup>33</sup> are also potential ways phagocytic myeloid cells can uptake components of live MSCs. After efferocytosis, trogocytosis, and paracytophagy cargo is encapsulated in intracellular vesicles with lipid bilayers. Either secondary signaling pathways in response to the process itself could be activated or intracellular cargo would need to be released from the vesicle to directly initiate signaling pathways. Tunneling nanotubes (TNTs) have been described in MSCs and macrophages and offer an alternative pathway. TNTs are cellular extensions that enable the transfer of cytosolic material from one cell to another cell through direct contact. A substantial amount of cytoplasmic cargo can be transferred through TNTs and they even demonstrated the ability to support transfer of RNA and large organelles such as mitochondria from MSCs to macrophages.<sup>29,34,35</sup> Formation of TNTs and transfer of cargo from MSCs increased the phagocytotic activity of macrophages.<sup>29</sup>

After monocytes and macrophages engulf components of hCT-MSCs, they undergo transcriptional changes and continue to suppress T cells even when hCT-MSCs are no longer present (Figure 2G). Monocytes and macrophages that engulf components of hCT-MSCs downregulated genes responsible for presenting antigens and activating T cells, including disease gene sets implicated in rheumatoid arthritis and primary immunodeficiencies (Figures 3B-F and 6C). Using a combination of computational and pharmacological approaches, we were able to inhibit the transfer of Qtracker from hCT-MSCs to monocytes and macrophages using a pan LRP inhibitor (Figure 4). LRPs are endocytic receptors that not only control the uptake of lipoproteins but are also involved in clearing dead cells and modulating the inflammatory response.<sup>36-38</sup> For example, deleting LRP expression on microglia (the brain's resident macrophages) enhanced pro-inflammatory cytokine secretion.<sup>39,40</sup> Our study suggests LRP mediates cell-to-cell interaction between hCT-MSCs and monocytes and macrophages which results in reprogramming monocytes and macrophages to inhibit the activation of T cells. Considering its main function, LRP would function in the monocytes and macrophages membrane to initiate the uptake of cytoplasmic components of hCT-MSCs. Once engaged through LRPs, MSCs would need to transfer signals to monocytes and macrophages through cytoplasmic components. Since a large amount of transcriptional information can be packaged in cytoplasmic p-bodies, and p-bodies are necessary for the epithelial-to-mesenchymal transition,<sup>41,42</sup> we first stained hCT-MSCs with DCP1A and DDX6 and found p-bodies to be abundant (Figure 5A). P-bodies are membrane-less, liquid-liquid phase cytoplasmic organelles that contain RNAs and RNA-binding proteins.<sup>42</sup> P-Bodies were initially thought to sequester mRNAs during stress; however, they have now been shown to play a role in translation under homeostasis, such as in synaptic plasticity.<sup>43</sup> Over 33% of

all coding mRNA can be packaged into p-bodies<sup>42</sup> and the RNA is enriched for control regulatory functions.<sup>44</sup>

Moreover, *in vitro* experiments revealed that formation of p-bodies is critical to suppress inflammatory cytokine expression in endotoxin tolerant macrophages.<sup>45</sup> When we genetically removed p-bodies in hCT-MSCs by deleting DDX6 via Crispr/Cas9, DDX6-KO hCT-MSCs failed to reprogram monocytes and macrophages and suppress T<sub>H</sub> cells *in vitro* (Figure 5D-G). *in vivo* data using an LPS-induced lung inflammation model demonstrated that DDX-KO hCT-MSC lost their ability to suppress inflammation and decrease the surface expression of MHC class II on infiltrating monocytes and macrophages that engulfed MSCs (Figure 6C). Deleting DDX6 did not prevent macrophages from engulfing cytoplasmic components of hCT-MSCs (Figures S7A and S8B). Our data suggest a novel mechanism regarding how MSCs can program monocytes and macrophages to inhibit T<sub>H</sub> cell activation and proliferation, which can explain long-term effects from MSC even after they are cleared.

## 5 | CONCLUSION

We report a novel mechanism of how hCT-MSCs reprogram monocytes and macrophages to suppress the activation of T<sub>H</sub> cells. hCT-MSCs directly contact monocytes and macrophages and transfer cytoplasmic components. The transfer of cytoplasmic material was dependent on LRP on the surface of monocytes and macrophages and processing bodies in hCT-MSCs. Monocytes and macrophages that engulfed hCT-MSC downregulated genes in antigen presentation and costimulatory pathways and could suppress the activation of T cells after hCT-MSCs were no longer present. These data could explain how MSCs have long-lasting beneficial effects *in vivo* despite being cleared hours after administration.

## ACKNOWLEDGMENTS

The authors thank all members of the Filiano lab and Marcus Center for Cellular Cures (MC3) for their valuable discussions through the project. This work was supported by grants from the Marcus Foundation (to Joanne Kurtzberg) and the Cord Blood Association (to Anthony J. Filiano). The graphical abstract was created using BioRender.

## CONFLICT OF INTEREST

T.K.T. declared an advisory role with Thermo Fisher Scientific. J.K. declared a leadership position with CryoCell and multiple IDFs filed at Duke for use of human cord tissue MSCs. The other authors declared no potential conflicts of interest.

## AUTHOR CONTRIBUTIONS

H.M., A.J.F.: designed and performed experiments, analyzed data, manuscript writing; L.X., R.P., C.C.O., M.L.: performed experiments, analyzed data, manuscript editing; E.M.R., R.R.R., T.K.T., A.F.C., A.G., J.K.: assisted with experimental design, manuscript editing; N.M.: oversaw manufacturing of hCT-MSCs.

## DATA AVAILABILITY STATEMENT

The data that support the findings of this study are available from the corresponding author upon reasonable request. Sequencing data has been uploaded to the GEO repository under accession no. GSE149848.

## ORCID

Teresa K. Tarrant  <https://orcid.org/0000-0003-4067-5363>

Anthony J. Filiano  <https://orcid.org/0000-0003-4329-0151>

## REFERENCES

- Galipeau J, Sensebe L. Mesenchymal stromal cells: clinical challenges and therapeutic opportunities. *Cell Stem Cell*. 2018;22(6):824-833.
- Uccelli A, Moretta L, Pistoia V. Mesenchymal stem cells in health and disease. *Nat Rev Immunol*. 2008;8(9):726-736.
- Liu Y, Mu R, Wang S, et al. Therapeutic potential of human umbilical cord mesenchymal stem cells in the treatment of rheumatoid arthritis. *Arthritis Res Ther*. 2010;12(6):R210.
- Francois M, Romieu-Mourez R, Li M, Galipeau J. Human MSC suppression correlates with cytokine induction of indoleamine 2,3-dioxygenase and bystander M2 macrophage differentiation. *Mol Ther*. 2012;20(1):187-195.
- Kota DJ, Prabhakara KS, Toledano-Furman N, et al. Prostaglandin E2 indicates therapeutic efficacy of mesenchymal stem cells in experimental traumatic brain injury. *STEM CELLS*. 2017;35(5):1416-1430.
- de Witte SFH, Luk F, Sierra Parraga JM, et al. Immunomodulation by therapeutic mesenchymal stromal cells (MSC) is triggered through phagocytosis of MSC by Monocytic cells. *STEM CELLS*. 2018;36(4):602-615.
- Galleu A, Riffo-Vasquez Y, Trento C, et al. Apoptosis in mesenchymal stromal cells induces in vivo recipient-mediated immunomodulation. *Sci Transl Med*. 2017;9(416):eaam7828.
- Cutler AJ, Limbani V, Girdlestone J, Navarrete CV. Umbilical cord-derived mesenchymal stromal cells modulate monocyte function to suppress T cell proliferation. *J Immunol*. 2010;185(11):6617-6623.
- Bolger AM, Lohse M, Usadel B. Trimmomatic: a flexible trimmer for Illumina sequence data. *Bioinformatics*. 2014;30(15):2114-2120.
- Andrews S. FastQC: a quality control tool for high throughput sequence data. Babraham Bioinformatics version 0.11.7; 2010. <https://www.bioinformatics.babraham.ac.uk/projects/fastqc/>
- Harrow J, Frankish A, Gonzalez JM, et al. GENCODE: the reference human genome annotation for the ENCODE project. *Genome Res*. 2012;22(9):1760-1774.
- Patro R, Duggal G, Love MI, Irizarry RA, Kingsford C. Salmon provides fast and bias-aware quantification of transcript expression. *Nat Methods*. 2017;14(4):417-419.
- Soneson C, Love MI, Robinson MD. Differential analyses for RNA-seq: transcript-level estimates improve gene-level inferences. *F1000Res*. 2015;4:1521.
- Love MI, Huber W, Anders S. Moderated estimation of fold change and dispersion for RNA-seq data with DESeq2. *Genome Biol*. 2014;15(12):550.
- Yu G, Wang LG, Han Y, He QY. clusterProfiler: an R package for comparing biological themes among gene clusters. *OmicS*. 2012;16(5):284-287.
- Ashburner M, Ball CA, Blake JA, et al. Gene ontology: tool for the unification of biology. The gene ontology consortium. *Nat Genet*. 2000;25(1):25-29.
- The Gene Ontology Consortium. Expansion of the gene ontology knowledgebase and resources. *Nucleic Acids Res*. 2017;45:D331-D338.
- Kanehisa M. Toward understanding the origin and evolution of cellular organisms. *Protein Sci*. 2019;28(11):1947-1951.
- Kanehisa M, Goto S. KEGG: kyoto encyclopedia of genes and genomes. *Nucleic Acids Res*. 2000;28(1):27-30.
- Kanehisa M, Sato Y, Furumichi M, Morishima K, Tanabe M. New approach for understanding genome variations in KEGG. *Nucleic Acids Res*. 2019;47(D1):D590-D595.
- Ley K, Pramod AB, Croft M, Ravichandran KS, Ting JP. How mouse macrophages sense what is going on. *Front Immunol*. 2016;7:204.
- Morioka S, Maueroder C, Ravichandran KS. Living on the edge: efferocytosis at the Interface of homeostasis and pathology. *Immunity*. 2019;50(5):1149-1162.
- Herz J, Goldstein JL, Strickland DK, Ho YK, Brown MS. 39-kDa protein modulates binding of ligands to low density lipoprotein receptor-related protein/alpha 2-macroglobulin receptor. *J Biol Chem*. 1991;266(31):21232-21238.
- Ayache J, Bénard M, Ernault-Lange M, et al. P-body assembly requires DDX6 repression complexes rather than decay or Ataxin2/2L complexes. *Mol Biol Cell*. 2015;26(14):2579-2595.
- Heathman TR, Nienow AW, McCall MJ, Coopman K, Kara B, Hewitt CJ. The translation of cell-based therapies: clinical landscape and manufacturing challenges. *Regen Med*. 2015;10(1):49-64.
- Kim J, Hematti P. Mesenchymal stem cell-educated macrophages: a novel type of alternatively activated macrophages. *Exp Hematol*. 2009;37(12):1445-1453.
- Melief SM, Schrama E, Brugman MH, et al. Multipotent stromal cells induce human regulatory T cells through a novel pathway involving skewing of monocytes toward anti-inflammatory macrophages. *STEM CELLS*. 2013;31(9):1980-1991.
- Nemeth K, Leelahavanichkul A, Yuen PST, et al. Bone marrow stromal cells attenuate sepsis via prostaglandin E(2)-dependent reprogramming of host macrophages to increase their interleukin-10 production. *Nat Med*. 2009;15(1):42-49.
- Jackson MV, Morrison TJ, Doherty DF, et al. Mitochondrial transfer via tunneling nanotubes is an important mechanism by which mesenchymal stem cells enhance macrophage phagocytosis in the in vitro and in vivo models of ARDS. *STEM CELLS*. 2016;34(8):2210-2223.
- Joly E, Hudrisier D. What is trogocytosis and what is its purpose? *Nat Immunol*. 2003;4(9):815.
- Spees JL, Olson SD, Whitney MJ, Prockop DJ. Mitochondrial transfer between cells can rescue aerobic respiration. *Proc Natl Acad Sci USA*. 2006;103(5):1283-1288.
- Robbins JR, Barth AI, Marquis H, de Hostos EL, Nelson WJ, Theriot JA. *Listeria monocytogenes* exploits normal host cell processes to spread from cell to cell. *J Cell Biol*. 1999;146(6):1333-1350.
- Rustom A, Saffrich R, Markovic I, Walther P, Gerdes HH. Nanotubular highways for intercellular organelle transport. *Science*. 2004;303(5660):1007-1010.
- Ariazi J, Benowitz A, de Biasi V, et al. Tunneling nanotubes and gap junctions-their role in long-range intercellular communication during development, health, and disease conditions. *Front Mol Neurosci*. 2017;10:333.
- Haimovich G, Ecker CM, Dunagin MC, et al. Intercellular mRNA trafficking via membrane nanotube-like extensions in mammalian cells. *Proc Natl Acad Sci USA*. 2017;114(46):E9873-E9882.
- Lillis AP, Muratoglu SC, Au DT, et al. LDL receptor-related protein-1 (LRP1) regulates cholesterol accumulation in macrophages. *PLoS One*. 2015;10(6):e0128903.
- Luo L, Wall AA, Tong SJ, et al. TLR crosstalk activates LRP1 to recruit Rab8a and PI3Kgamma for suppression of inflammatory responses. *Cell Rep*. 2018;24(11):3033-3044.
- Gardai SJ, McPhillips KA, Frasch SC, et al. Cell-surface calreticulin initiates clearance of viable or apoptotic cells through trans-activation of LRP on the phagocyte. *Cell*. 2005;123(2):321-334.
- May P, Bock HH, Nofer JR. Low density receptor-related protein 1 (LRP1) promotes anti-inflammatory phenotype in murine macrophages. *Cell Tissue Res*. 2013;354(3):887-889.

40. Yang L, Liu CC, Zheng H, et al. LRP1 modulates the microglial immune response via regulation of JNK and NF-kappaB signaling pathways. *J Neuroinflammation*. 2016;13(1):304.
41. Hardy SD, Shinde A, Wang WH, Wendt MK, Geahlen RL. Regulation of epithelial-mesenchymal transition and metastasis by TGF-beta, P-bodies, and autophagy. *Oncotarget*. 2017;8(61):103302-103314.
42. Standart N, Weil D. P-bodies: cytosolic droplets for coordinated mRNA storage. *Trends Genet*. 2018;34(8):612-626.
43. Oh JY, Kwon A, Jo A, et al. Activity-dependent synaptic localization of processing bodies and their role in dendritic structural plasticity. *J Cell Sci*. 2013;126(Pt 9):2114-2123.
44. Hubstenberger, A., Courel M., Bénard M., et al. P-body purification reveals the condensation of repressed mRNA regulons. *Mol Cell*. 2017. 68(1): p. 144-157.e5
45. McClure C, Brudecki L, Yao ZQ, McCall CE, el Gazzar M. Processing body formation limits proinflammatory cytokine synthesis in

endotoxin-tolerant monocytes and murine septic macrophages. *J Innate Immun*. 2015;7(6):572-583.

#### SUPPORTING INFORMATION

Additional supporting information may be found online in the Supporting Information section at the end of this article.

**How to cite this article:** Min H, Xu L, Parrott R, et al. Mesenchymal stromal cells reprogram monocytes and macrophages with processing bodies. *Stem Cells*. 2021;39: 115-128. <https://doi.org/10.1002/stem.3292>